Progress In Electromagnetics Research C, Vol. 21, 191–203, 2011

COMBINING DIFFERENT IN-PLANE PHOTONIC WIRE LASERS AND COUPLING THE RESULTING FIELD INTO A SINGLE-MODE WAVEGUIDE

M. Rezaur Raihan[1, *], Z. Li[1], D. Liu[2], H. T. Hattori[1], and M. Premaratne[3]

[1]School of Engineering and Information Technology, University of New South Wales, Australian Defence Force Academy, Canberra, ACT 2600, Australia

[2]Research School of Physics and Engineering, Australian National University, Canberra, ACT 0200, Australia

[3]Advanced Computing and Simulation Laboratory (AXL), Department of Electrical and Computer Systems Engineering, Monash University, Clayton, VIC 3800, Australia

Abstract—Photonic wire lasers are compact light sources that are fabricated in high-index contrast waveguides (with typical widths of a few hundreds of nanometers). Because of their small footprints, they may become a basic laser component in future-generation of optical integrated circuits. Owing to having low optical volume by design, photonic wire lasers can only produce low output power that may not be adequate in many applications. A solution to this problem is to coherently combine the output power of different photonic wire lasers to produce larger output power. In this article, we analyze different ways to combine light coming out from photonic wire lasers and couple the combined power into a single-mode waveguide.

1. INTRODUCTION

Electronics has revolutionized the way people handle and exchange data and information. This revolution has become possible because large amounts of data can be manipulated and processed by very tiny electronic circuits. In contrast, optical circuits are significantly

Received 21 November 2010, Accepted 9 May 2011, Scheduled 12 May 2011

* Corresponding author: Md. Rezaur Raihan (Md.Raihan@student.adfa.edu.au).

larger than their electronic counterparts, although they can potentially operate at much higher speeds. Future generation of integrated circuits may combine the advantages of both technologies, resulting in the creation of hybrid opto-electronic integrated circuits. However, for this combination of technologies to occur, optical circuits will need to significantly reduce their sizes to operate side by side with their electronic counterparts.

The prospect of creating hybrid high speed and compact opto-electronic devices brings the issue of confining and manipulating light at the micrometer and nanometer scale. Nowadays, there are different physical phenomena that can be used to confine light at the micrometer/sub-micrometer scale such as the photonic bandgap effect [1–7], total internal reflection [8–11] and plasmonic propagation [12–17]. An example of compact device based upon total internal reflection is the photonic wire [18]: they have widths in the range of a few hundreds of nanometers and light is confined laterally by total internal reflection at the boundaries between the core and low refractive-index air layers. On the other hand, in photonic bandgap devices, light is confined in a region surrounded by periodic structures with different refractive indices that operate in their bandgap region: in this wavelength range, light is forbidden to propagate along certain directions. A combination of photonic crystal and photonic wires can produce highly compact devices [19] where not only light is concentrated in small regions but the actual volumes of the devices are also small (the lateral confinement of light is due to total internal reflection: not many periods of the photonic crystal is necessary to confine light laterally).

However, coupling of light to and from these devices is not trivial and requires a detailed analysis. To gain insight into such designs, in this article, we start from a basic photonic wire laser device. Then, the basic device is modified to improve its performance without significantly increasing its size (volume). Finally, different ways to combine similar photonic wire laser devices to produce a higher output power are presented. The significance of such power combining can be seen by noting that a single photonic wire laser may not produce a large output power because of its reduced dimensions. Very low generated power may hinder certain applications where medium amounts of power are needed. In these applications, these miniature lasers could only be useful if several devices are put together to produce high output as demonstrated in this paper. Our aim is to show key considerations required to carry-out such integration and provide valuable insight to designers.

2. EXAMPLE SYSTEM: GaAs/INGaAs PHOTONIC WIRE LASER

In order to illustrate the main ideas in combining and subsequently coupling light into a single photonic wire waveguide, the epitaxially layered structure shown in Figure 1(a) is employed. It consists of a core layer of GaAs with three 7.3 nm thick $In_{0.2}Ga_{0.8}As$ quantum wells, separated by 6 nm GaAs confinement barriers. The thickness of the core layer is 140 nm. In this epitaxially grown layer, the photonic wire lasers will be fabricated. In order to confine light vertically, the whole structure is assumed to be in a suspended membrane [19, 20]. In principle, many other multi-layered structures could be used to confine light vertically. For example, the bottom cladding layers could consist of an oxidized $Al_{0.98}Ga_{0.02}As$ layer or a Bragg stack with alternating quarter wavelength optical materials. In this article, the suspended membrane structure is designed to operate with TE modes that have the main component of the magnetic field perpendicular to the plane of the device (y-direction, H_y). The quantum wells are grown to emit light primarily at the free-space wavelength (λ) of 980 nm, with a gain linewidth of 40 nm.

In order to analyze these devices, commercial 2D Finite Difference Time Domain (FDTD) software [21] is used. A source is placed at the center of the laser cavity with a spot size diameter matched to the waveguide. The effective index of the slab structure is 2.86. The computation region is terminated by perfectly matched absorbing

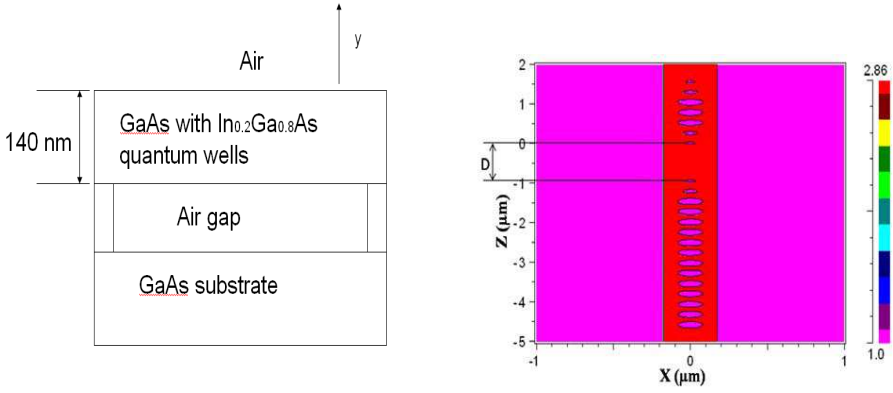

Figure 1. (a) Epitaxially layered structure of the photonic wire lasers. (b) Top view of a photonic wire laser.

layers. The grid specified in the calculations is uniform along the x and z directions, (with grid sizes $\Delta x = \Delta z = 30\,\text{nm}$) and the time step is chosen as $\Delta t = 3.53 \times 10^{-17}\,\text{s}$. At this stage, no material gain is added to the simulations, since parameters such as transmission through the waveguides are being assessed and, in many times, the addition of material gain can lead to numerical instabilities in the FDTD codes.

A basic photonic wire laser is shown in Figure 1(b). In Figure 1(b), the red color represents the solid material while the pink color represents the air regions. Cylindrical air holes are etched into the single-mode waveguide of width of 350 nm. A 'solid' defect is introduced in this sequence of air holes to create a cavity. The distance between the tiny central holes is $D = 0.95\,\mu\text{m}$ (this separation creates a 'solid' defect in the periodic structure that forms the laser cavity). The larger holes have diameters of 160 nm. In Figure 1(b), the two holes closer to the center of the cavity have a diameter of 60 nm and are followed by holes of diameter of 90 nm. In the region $z < -1\,\mu\text{m}$, the holes are large and have a diameter of 160 nm: these large holes are intended to block most of the light going into the $z < 0$ direction, concentrating the emitted light in the forward direction ($z > 0$). In the forward direction ($z < 0$), one hole has a diameter of 60 nm, another hole a diameter of 90 nm, three holes a diameter of 160 nm, one hole a diameter of 90 nm and a final hole a diameter of 60 nm. The lattice constant of this one-dimensional photonic crystal used for the laser is 260 nm. These dimensions are chosen to optimize the transmission through the waveguide in the forward direction and, at the same time, obtain high quality factors for the resonant modes. On the other hand, the distance is chosen to be as large as possible to provide a reasonable amount of output power, but at the same time, to have only a single-mode in the gain region of the quantum wells.

Magnetic field (H_y) spectrum at the center of the waveguide (outside the cavity region, i.e., $z > 3\,\mu\text{m}$) is shown in Figure 2(a). In the wavelength region between 910 nm and 1060 nm, the resonant wavelength peaks and their associated quality factors (Qs) are: 923.01 nm ($Q = 367$), 987.82 nm ($Q = 1085$) and 1079.3 nm ($Q = 1542$). Although there are many resonant peaks, only the resonant peak which is located at 987.82 nm is in the narrow gain region of the quantum wells. This means that, essentially, only this peak can reach lasing in this device. A power budget analysis indicates that, at this peak, about 98% of the generated power is transmitted in the forward direction ($z > 0$) of the single-mode waveguide.

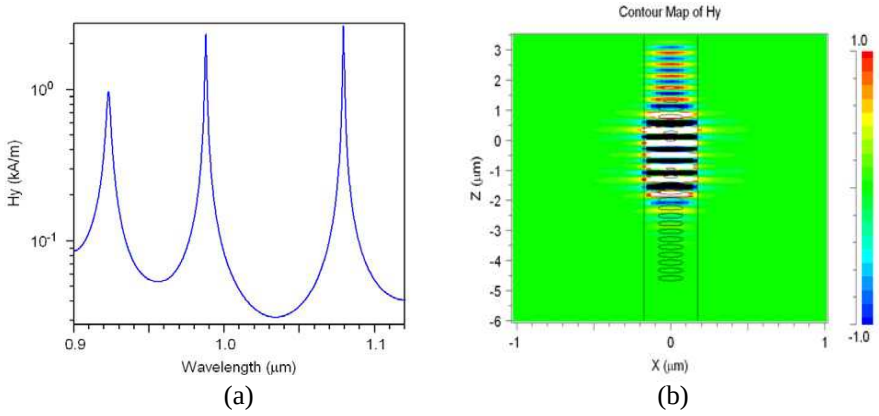

Figure 2. Basic photonic wire laser: (a) Magnetic field spectrum (H_y) at the center of the waveguide. (b) Magnetic field (H_y) distribution at $\lambda = 987.82\,\text{nm}$.

3. COMBINING DIFFERENT PHOTONIC WIRE LASERS

The power coming out from these tiny lasers is small. In some applications, more power from these lasers is required. In these situations, power coming out from different lasers can be combined and coupled into a single-mode waveguide by using power combiners. In order to design these combiners, it is initially assumed that light coming out from the lasers have the same phase and power.

The first proposed power combiner is a multimode interference coupler as shown in Figure 3(a). The lasers are separated by 800 nm, so that there is a weak coupling between adjacent laser devices. The width of the coupler is assumed to be 1.95 μm. In order to calculate how much power is injected into the single-mode waveguide, individual sources are placed in the photonic wire cavities: the sources have the same phase, amplitude and positioned at the same z-coordinate. For a length of 3.74 μm of the coupler the efficiency is found to be 30% from the power budget analysis. But if the laser at the center of the array is displaced in the forward z-direction, the efficiency increases significantly. For a displacement of 260 nm the efficiency rises to 70% for the same length of the coupler. Figure 3(b) shows the coupling efficiency of the coupler as a function of its length L_1 (at the resonant wavelength of 987.82 nm). In order to understand this behavior, it is necessary to consider that there is an interference between the three waves coming from the three photonic wire lasers and that there will

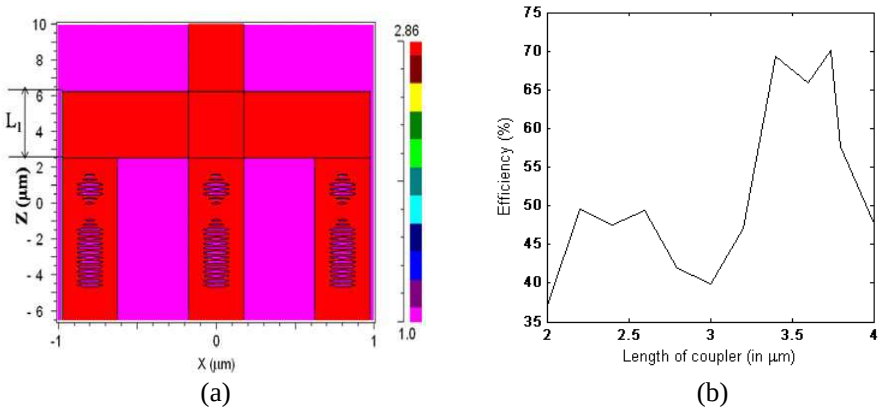

Figure 3. (a) Multimode interference coupler used to combine the power coming from three different photonic wire sources. (b) Coupling efficiency as a function of the length of the coupler.

be a maximum constructive interference for an optimum value. To get a maximum constructive interference the coupler length, the relative power and phase between the laser at $x = 0$ and the lasers at the far left and right of the coupler should be optimized, i.e., they must reach the single-mode waveguide in a constructive way. It may be somewhat difficult to get exact relative phase between the laser at $x = 0$ and the lasers at the far left and right of the coupler, so an option to move the position of the laser in the z-direction is chosen and the relative position is optimized. From this plot, it is clear that the maximum coupling efficiency is 70% for a coupler length $L_1 = 3.74\,\mu\text{m}$. The coupling efficiency is not 100% because of radiation losses. Light leaks away in different directions, but apparently light escaping in the lateral directions of the multimode interference coupler is the main source of power loss.

To reduce the power losses in the lateral directions a coupler which is composed of a multimode interference coupler along with triangular lattice of holes as shown in Figure 4(a) is proposed. Eight columns of air holes are placed on each side of the multimode interference coupler. The lattice constant is 300 nm and the photonic crystal operates in its bandgap region at the wavelength of 987.82 nm. The radius of the air holes result in a filling factor of 40%. The central laser is displaced by 260 nm in the forward z-direction with respect to the lasers at the edge of the array. For these settings, a coupling efficiency of 82% is obtained. Figure 4(b) shows the magnetic field distribution (H_y) for the optimized combiner of the three photonic wire lasers. The addition

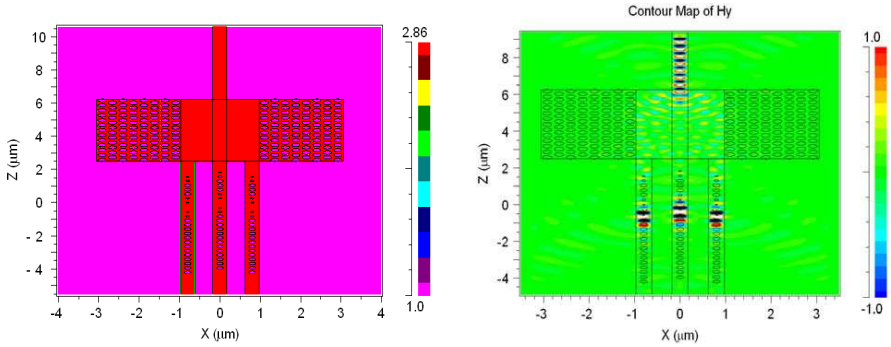

Figure 4. (a) Triangular array of holes added to multimode interference coupler to improve the total power in the single mode waveguide. (b) Magnetic field (H_y) distribution at $\lambda = 987.82$ nm for the optimized combiner.

of the photonic crystal surrounding the multimode interference coupler does not change the resonant wavelength of the laser and increase the coupling efficiency to 82%. The remaining 18% is lost through radiation as can be observed in Figure 4(b). Moreover, after light is coupled into the single-mode waveguide, a small portion still escapes away from the waveguide.

Another aspect that is further exploited is the effects of the relative positions and amplitudes of the lasers on the coupling efficiency. Figure 5(a) shows the effects of the positions of the lasers at the far right and left of the optimized combiner with respect to the position of the laser located at $x = 0$ (it is assumed that the lasers located at the extreme left and right of the coupler have the same position). From Figure 5(a), it is clear that the worst coupling efficiency occurs when all lasers are aligned to each other. The coupling efficiency is maximum for a relative change in position of 260 nm. In fact, this relative position can be changed from 200 nm to 320 nm without significant change in coupling efficiency. High spatial frequency oscillations seem to be present in Figure 5(a). These oscillations are numerical artifacts of the FDTD method that can be reduced by decreasing the step-size, grid sizes in the x and z directions. However, the reduction of the grid sizes comes at the expense of the much longer simulation time.

Figure 5(b) exploits the effect of the relative power between the lasers at extreme left and right of the coupler (assumed to have same power P_1) and the central laser (assumed to have power P_0). Again, the coupling efficiency is not significantly degraded when P_1/P_0

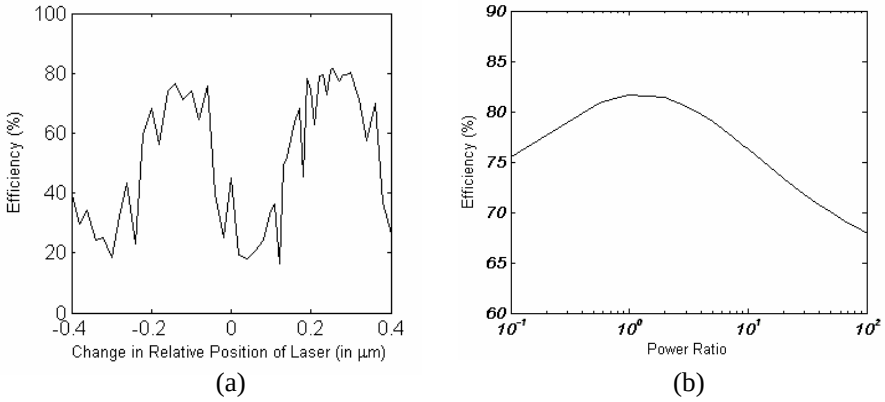

Figure 5. Multimode interference coupler with triangular array of holes: (a) Coupling efficiency as a function of the relative position among the sources of lasers and (b) coupling efficiency as a function of the relative power between the lasers for the optimized combiner.

changes from the optimum value of 1.0. Close to the edges of the combiner, it would be expected that the radiation losses would be higher; in spite of higher radiation losses, the combiner is still capable of combining a significant amount of the emitted power into the single-mode waveguide.

In this article, three lasers are used to merge to produce higher output power. Not many lasers were combined to allow a better understanding of the physical phenomena behind the combination of power from different lasers. If more lasers are to be combined, then different combiners can be used to combine lasers in groups of three and then use other combiners to further combine the power coming from different combiners. This approach is called "tree-structure" that is widely used in systems engineering. Using this method we combined power from 9 lasers to a single mode waveguide. Each group of three lasers was combined using the coupler described before and then another coupler was used to couple the output of those three couplers as shown in Figure 6. The output of the couplers which are at the left and right side of the middle need a bend to further feed this power to another coupler, leading to a different path length for the couplers at the edge. After the optimization of the complete structure, an overall efficiency of 62% was obtained with additional radiation losses because of the introduction of additional couplers.

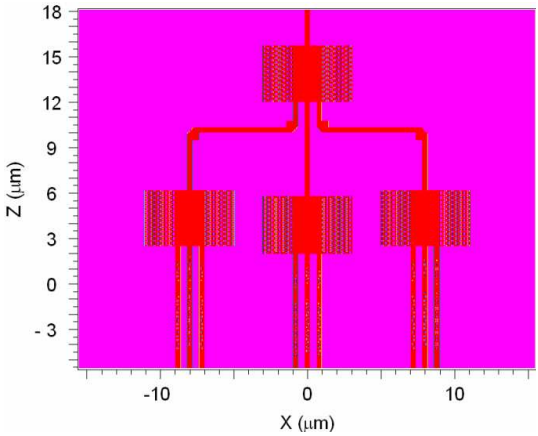

Figure 6. Array of 9 laser coupled by four multimode interference coupler with triangular array of holes to couple the resulting field to asingle mode waveguide.

4. INJECTION LOCKING THE LASERS

So far in the paper, it was assumed that the lasers were coherent and there was no phase difference among the fields produced by the lasers. In order to achieve this goal one common approach is to use injection locking. In injection locking, if the frequency of a free running slave laser is close enough to the master laser frequency; the slave will lase at the same frequency as the injected master beam. Within the locking range, both lasers run coherently with the same frequency and a stable phase relation. In this paper, the locking of two lasers is analyzed. The procedure could be extended to more lasers, but is out of scope of this paper.

The differential equation governing the complex field of an injection-locked laser is similar to that of a free-running laser, with the addition of an injection term [22]

$$\frac{dE(t)}{dt} = \frac{1}{2}g\Delta N(1+j\alpha)E(t) + \kappa A_{inj} - j\Delta\omega_{inj}E(t) \qquad (1)$$

where $E(t)$ is the slave laser's complex field. This model ignores spontaneous emission and noise. This equation can be split into the field magnitude and phase by assuming that $E(t) = A(t)\exp j\phi(t)$. The split equation, along with the carrier rate equation, constitute the

three differential equations of injection-locked lasers [23]

$$\frac{dA(t)}{dt} = \frac{1}{2}g[N(t) - N_{th}]A(t) + \kappa A_{inj}\cos\phi(t) \quad (2)$$

$$\frac{d\phi(t)}{dt} = \frac{\alpha}{2}g[N(t) - N_{th}] - \kappa\frac{A_{inj}}{A(t)}\sin\phi(t) - \Delta\omega_{inj} \quad (3)$$

$$\frac{dN(t)}{dt} = J - \gamma_N N(t) - \{\gamma_p + g[N(t) - N_{th}]\}A(t)^2 \quad (4)$$

where $A(t)$, $\phi(t)$ and $N(t)$ are the slave laser's field magnitude, field phase, and carrier number. $A(t)$ is normalized as $A^2(t) = S(t)$, where $S(t)$ is the photon number and $\phi(t)$ is the phase difference between master and slave: $\phi(t) \equiv \phi_{slave}(t) - \phi_{master}(t)$. The parameters g, N_{th}, α, J, γ_N, and γ_P are the slave laser's linear gain coefficient, threshold carrier number, linewidth enhancement factor, current, carrier recombination rate, and photon decay rate, respectively. The injection terms, κ, A_{inj}, and $\Delta\omega_{inj}$ are the coupling rate, injected field magnitude, and detuning frequency, respectively. The detuning frequency is defined as the difference between master and free-running slave frequencies.

Equations (2) to (4) are solved analytically by using perturbation methods, following the approach described in [24]. The results are shown in Figure 7(a). The two lasers will be unlocked in a small

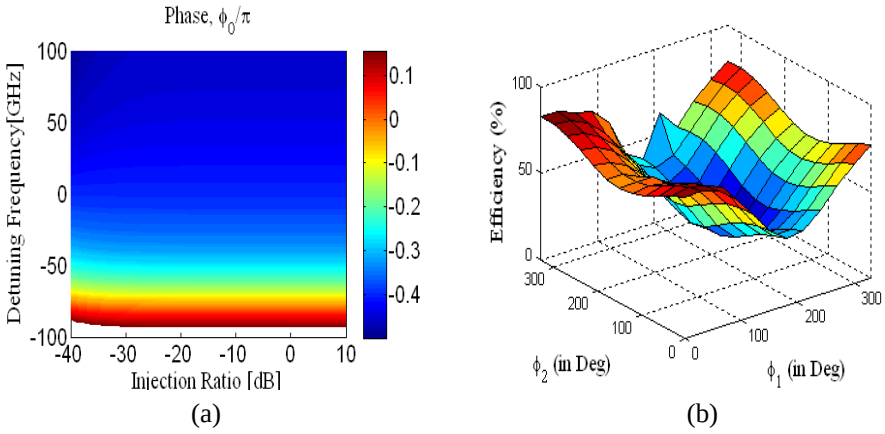

Figure 7. (a) The contour map showing the phase difference between master and slave laser for different values of injection ratio and detuning frequency. (b) Coupling efficiency as a function of the difference in phase from the middle laser to the lasers at the right and left.

region in Figure 7(a), i.e., for a detuning frequency below −90 GHz and above 100 GHz. On the other hand, they are locked over a wide range of injection ratio and strongly locked in the region −70 GHz $< \Delta f_{inj} <$ −90 GHz. The effects of the relative phase between different lasers are examined in Figure 7(b). The laser in the middle of the array is assumed to have a phase of 0°, while the relative phase of the right and left lasers are ϕ_1 and ϕ_2, respectively. The middle laser is also displaced by 260 nm in the forward z direction as discussed previously. There are many maxima for the coupling efficiency. For example, when $\phi_1 = \phi_2 = 0°$, the coupling efficiency is 82%, the lowest coupling efficiency is 20% and it occurs when $\phi_1 = 180°$ and $\phi_2 = 150°$ (the lasers at the edge are nearly out of phase with respect to the laser in the center).

5. CONCLUSIONS

In this article, we presented combiners that could merge the power coming out from three different photonic wire lasers into a single-mode waveguide. The combination of a multimode interference coupler and a photonic crystal cladding resulted in a coupling efficiency of 82%. The coupling efficiency doesn't vary considerably with changes of the relative powers of different photonic wire lasers. However, the relative position of the laser critically influences the coupling efficiency of the lasers with tolerance of ±60 nm.

ACKNOWLEDGMENT

The authors gratefully acknowledge the financial support to this project by the Australian Research Council (ARC).

REFERENCES

1. Painter, O., R. K. Lee, A. Scherrer, A. Yariv, J. D. O'Brien, and P. D. Dapkus, "Two-dimensional photonic bandgap defect mode laser," *Science*, Vol. 284, 1819–1821, 1999.
2. Park, H. G., J. K. Hwang, J. Huh, H. Y. Ryu, S. H. Kim, J. S. Kim, and Y. H. Lee, "Characteristics of modified single-defect two-dimensional photonic crystal lasers," *IEEE J. Quantum Electron.*, Vol. 38, 1353–1365, 2002.
3. Song, D. S., S. H. Kim, H. G. Park, C. K. Kim, and Y. H. Lee, "Single-fundamental-mode photonic crystal surface-emitting lasers," *Appl. Phys. Lett.*, Vol. 80, 3608–3610, 2003.

4. Hattori, H. T., C. Seassal, X. Letartre, P. Rojo-Romeo, J. L. Leclercq, P. Viktorovitch, M. Zussy, L. di Cioccio, L. El Melhaoui, and J. M. Fedeli, "Coupling analysis of heterogeneous integrated InP based photonic crystal triangular lattice band-edge lasers and silicon waveguides," *Opt. Express*, Vol. 13, 3310–3322, 2005.
5. Amaratunga, V. S., H. T. Hattori, M. Premaratne, H. H. Tan, and C. Jagadish, "Photonic crystal phase detector," *J. Opt. Soc. Am. B*, Vol. 25, 1532–1536, 2008.
6. Matsumoto, T. and T. Baba, "Photonic crystal k-vector superprism," *J. Lightwave Technol.*, Vol. 22, 917–922, 2004.
7. Ohnishi, D., T. Okano, M. Imada, and S. Noda, "Room temperature continuous wave operation of a surface-emitting two-dimensional photonic crystal diode laser," *Opt. Express*, Vol. 12, 1562–1568, 2004.
8. Fujita, M., A. Sakai, and T. Baba, "Ultra-small and ultra-low threshold microdisk injection laser-design, fabrication, lasing characteristics and spontaneous emission factor," *IEEE J. Sel. Top. Quantum Electron.*, Vol. 5, 673–681, 1999.
9. Boriskina, S. V., T. M. Benson, P. D. Sewell, and A. I. Nosich, "Directional emission, increased free spectral range, and mode Q-factors in 2-D wavelength-scale optical microcavity structures," *IEEE J. Sel. Top. Quantum Electron.*, Vol. 12, 1175–1182, 2006.
10. Hattori, H. T., "Analysis of optically pumped equilateral triangular microlasers with three mode-selective trenches," *Appl. Optics*, Vol. 47, 2178–2185, 2008.
11. Hattori, H. T., D. Y. Liu, H. H. Tan, and C. Jagadish, "Large square resonator laser with quasi-single-mode operation," *IEEE Phot. Technol. Lett.*, Vol. 21, 359–361, 2005.
12. Genet, C. and T. W. Ebbesen, "Light in tiny holes," *Nature*, Vol. 445, 39–46, 2007.
13. Laux, E., C. Genet, T. Skauli, and T. W. Ebbesen, "Plasmonic photon sorters for spectral and polarimetric imaging," *Nature Phot.*, Vol. 2, 161, 2008.
14. Yu, N., E. Cubukcu, L. Diehl, M. A. Belkin, K. B. Crozier, F. Capasso, D. Bour, S. Corzine, and G. Hofler, "Plasmonic quantum cascade laser antenna," *Appl. Phys. Lett.*, Vol. 91, 173113, 2007.
15. Liu, D. Y., H. T. Hattori, L. Fu, H. H. Tan, and C. Jagadish, "Coupling analysis of GaAs-based microdisk lasers with different external claddings," *J. Lightwave Technol.*, Vol. 27, 5090–5098,

2009.

16. Hattori, H. T., Z. Li, D. Y. Liu, I. D. Rukhlenko, and M. Premaratne, "Coupling of light from microdisk lasers into plasmonic nano-antennas," *Opt. Express*, Vol. 17, 20878–20884, 2009.
17. Bogaerts, W., D. Tailaert, B. Luyssaert, P. Dumon, J. Van Campehout, P. Bientsman, D. Van Thourhout, R. Baets, V. Wiaux, and S. Beckx, "Basic structures for photonic integrated circuits in silicon-on-insulator," *Opt. Express*, Vol. 12, 1583–1591, 2004.
18. Zain, A. R., N. P. Johnson, M. Sorel, and R. M. De La Rue, "High quality-factor 1-D-suspended photonic crystal/photonic wire silicon waveguide micro-cavities," *IEEE Phot. Technol. Lett.*, Vol. 21, 1789–1791, 2009.
19. Homeyer, E., J. Houel, X. Checoury, G. Fishman, S. Sauvage, and P. Boucaud, "Thermal emission of midinfrared GaAs photonic crystal," *Phys. Rev. B*, Vol. 78, 165305, 2008.
20. Hascik, S., I. Hotovy, T. Lalinsky, G. Vanko, V. Rehacek, and Z. Mozolova, "Preparation of thin GaAs suspended membranes for gas micro-sensors using plasma etching," *Vacuum*, Vol. 82, 236–239, 2008.
21. Fullwave 4.0 RSOFT design group, http://www.rsoftdesign.com, 1999.
22. Henry, C., N. Olsson, and N. Dutta, "Locking range and stability of injection locked 1.54 μm InGaAsPSemiconductor lasers," *IEEE Journal of Quantum Electronics*, Vol. 21, 1152–1156, 1985.
23. Murakami, A., K. Kawashima, and K. Atsuki, "Cavity resonance shift and bandwidth enhancement in semiconductor lasers with strong light injection," *IEEE Journal of Quantum Electronics*, Vol. 39, 1196–1204, 2003.
24. Lau, E. K., S. Hyuk-Kee, and M. C. Wu, "Frequency response enhancement of optical injection-locked lasers," *IEEE Journal of Quantum Electronics*, Vol. 44, 90–99, 2008.